The Movement Process of Typical Slope Debris Flow: A Case Study of Wujia Gully, Zengda, Sichuan Province China

Shunyu Yao (yaoshunyu16@mails.ucas.edu.cn)

Institute of Geographic Sciences and Natural Resources Research CAS: Institute of Geographic Sciences and Natural Resources Research Chinese Academy of Sciences https://orcid.org/0000-0003-3399-8033

Bazai Nazir Ahmed

China-Pakistan Joint Research Center on Earth Sciences

Hu Jiang

Southwest University of Science and Technology

Shujian Yi

Institute of Mountain Hazards and Environment Chinese Academy of Sciences

Qiang Zou

Institute of Mountain Hazards and Environment Chinese Academy of Sciences

Tashfain Ahmed

Balochistan University of Information Technology Engineering and Management Sciences

Jian Guo

Chang'an University

Research Article

Keywords: Wujia gully debris flow, Topography, Shallow water equation, debris flow movement

Posted Date: October 27th, 2021

DOI: https://doi.org/10.21203/rs.3.rs-1002479/v1

Abstract

A debris flow occurred on July 25, 2020, at Wujia gully, Sichuan Province, China. The previous debris flow in Wujia gully happened 70 years ago. The debris flow had a severe impact downstream. The primary goal of this study is to comprehend the impact of debris flow topography on the movement process. This study compiles field data evidence from locals and conducts field sampling to get specific information using Unmanned Aerial Vehicle (UAV) aerial photography. The rheological properties of debris flow slurry are obtained through soil mechanics and rheological experiments. The movement process of the debris flow was simulated using the depth-integrated continuum approach. Based on numerical simulation analysis, the influence of Wujia gully topography on the debris flow movement process was examined. The analysis reveals that the debris flow in Wujia gully is a typical viscous debris flow, and the debris flow slurry matches the properties of Bingham fluid. Based on slope and elevation, the topography of the Wujia gully debris flow path may be classified into three sections: slope movement area, channel movement area, and deposition area. Furthermore, the topography is the most important element in debris flow movement. The consistent change in the velocity of debris flows on the topographical variation was observed, combined with the viscous debris flow and resistance characteristics. This study may serve as a reference for future debris flow kinematics research and a flow channel for researching typical slope debris flow and its movement process.

1 Introduction

Debris flow counts among one of the major mountain disasters in Western Sichuan (Wu et al. 2016). The Dadu River Basin is a high-incidence area of mountain disasters such as debris flow, landslides, and flash floods (Ji et al. 2020) (Ni et al. 2014), posing a considerable threat to riverside settlements. Mostly these settlements are built in front of debris-flow gulleys, and for a long time, due to the absence of debris flows, the awareness of these hazards for locals are not in their priority, and whenever the debris flow strikes, the reaction time is limited and consequently recorded massive losses. (Ji et al. 2020; Ni et al. 2014). There are many causes of debris flows(Cheng et al. 2018)(such as vegetation reduction(Vanmaercke et al. 2010), rainfalls (Cui et al. 2017), human activities(Preuth et al. 2010), river erosion(Lévy et al. 2012), earthquakes (Xiao et al. 2011), slope instability(F.C et al. 2002) and freeze-thaw (Deng et al. 2017)). Still, the movement of debris flow has an important impact on the formation of disasters. After the Wenchuan earthquake, the debris flowed in the Longxi River Basin on a large scale and created massive destruction to infrastructure, settlements, and farmlands(Chang et al. 2017; Ding et al. 2019). On August 7, 2010, a low-frequency debris flow in the Zhouqu, Gansu region occurred and killed 1,463 people (Zhao et al. 2020). Two channels converge into one channel, which significantly affects the movement of debris flow(Tang et al. 2011; Wang 2013; Zhang and Matsushima 2016). A massive ditch debris flow occurred in Gansu Province, China, in July 2013. The debris drifted downstream along the river when the channel took a severe curve. The debris flow jumped 1040 m and destroyed more than ten houses (Peng et al. 2014). The topography will significantly affect the movement process of the debris flow, thereby affecting the damage results of the debris flow(Iverson 2005).

In recent years, many studies on the kinematics characteristics of debris flow have been carried out, for example, by extracting topographic parameters (stream power index (SPI), topographic wetness index (TWI)) in the channels to study the movement characteristics or debris flow characteristics (Bhandari and Dhakal 2019; Chen and Lee 2010; Lee et al. 2015; Tie 2014). The method of extracting topographical factors is mainly used in the hazard assessment of debris flow. Usually, hope to find the relationship between the result of debris flow and topographical factors (Ali et al. 2021; Chen et al. 2020; Li et al. 2020; Liang et al. 2020a; Liang et al. 2020b; Liu et al. 2020; Sujatha 2020; Xiong et al. 2020; Zhao et al. 2020). This method extracts the factors such as slope and channel gradient as the evaluation factors of debris flow movement, and it is impossible to consider the movement process of debris flow.

Some people also set up experimental conditions (bed surface roughness, slope, etc.) to research the movement mechanism of debris flow (De Haas et al. 2015; Iverson 2003, 2005, 2015; Iverson et al. 2010a; Jian et al. 2018; Reid et al. 2011). On the other hand, traditional debris flow research simplifies complex topography by focusing on a single feature or a group of elements. Topography greatly influences debris flow movement, and only a few parameters cannot reflect the complex topography in nature. Numerical simulation is a standard method for simulating the complex topography movement process of debris flow. The main numerical simulation methods include DEM(Discrete Element Method)(Shen et al. 2018), SPH(Smoothed Particle Hydrodynamics)(Dai et al. 2017; Minatti and Pasculli 2011), and Continuum hypothetical depth integral numerical method (Iverson and Ouyang 2015; Ouyang et al. 2013). DEM and SPH are based on the hypothesis of material discrete and calculates the physical state of each particle through the constitutive stress model between particles. They are generally used to simulate particle fields, not suitable for simulating debris flow. The depth-integrated Navier-Stokes equation is now the most commonly used physical theoretical model to analyze debris flow movement based on the continuum assumption.

The Wujia gully debris flow occurred in Zengda, one tributary of Dadu River Basin in southwest China. Since July 25 2020, Wujia gully has continuously occurred three large-scale and dozens of small-scale debris flows. Because it has been a long time since the last debris flow outbreak, this form of debris flow is difficult to react to and plan for, and it is a high-risk type of debris flow. The Wujia gully debris flow has a characteristic slope and straight channel, which is favorable to inducing high-movement debris flow process. An in-depth study of the impact of topography on the movement process of debris flow is critical to the disaster reduction of abrupt debris flow that is likely to cause catastrophe, therefore this study selects Wujia gully as a case.

In the current research, field observation and numerical modelling were used to examine the influence of topography on the kinematics of the Wujia gully debris flow. Initially, the topography, geology, and meteorological conditions of Zengda were briefly introduced. Secondly, field survey, physical experiments, and the rheological parameters necessary for numerical modelling were used to examine the rheological properties of the debris flow. Furthermore, numerical simulation technique would also be used to determine the debris flow's momentum and flow depth on the Wujia gully’s slope during the acceleration,

channel migration, and the accumulation stages. Finally, the effect of Wujia gully topography on the different movement stages of debris flow is discussed.

2 Study Area

2.1 Topography and landform

Zengda is located in the section from Jinchuan to Danba in the Dadu River Basin, in the southwest of the Aba Tibetan and Qiang Autonomous Prefecture. It belongs to Sichuan Province(Statistics 2020) ; geographic coordinates extend 101°58’39.40 "E-102°8'6.79"E, 31°4'24.82" N-31°15'47.87"N (Fig. 1a-c). The research area lies on the eastern edge of the Qinghai-Tibet Plateau, with sky-high mountains, deep rivers, deep valleys, significant surface undulations, and significant elevation changes (Dai et al. 2005). With a drainage area of 155km^2, the whole Zengda watershed is a tributary of the Dadu River, with 13 debris flow ditches covering more than 3km^2. Wujia gully, which broke three times in a row this year, is one of them. It is 2321.60m, and the channel is a V-shaped channel with ratio 0.40, the source area is 3.5180km^2. Wujia gully is a typical low-frequency debris flow channel that has existed for at least 70 years since the previous debris flow eruption. The accumulation area is about 52113m^2, and a large area of arable land was buried after the eruption, causing damage to six houses.

2.2 Geological and climate setting

Figure 2a describes the Zengda debris flow in the Xiaojin arc tectonic system with relatively more folds and few faults. The study area consists mainly of Devonian to Triassic sediments, including quartzite, marble, sandstone, slate, etc (Figure 2a). Moreover, there are also some magmatic rocks and Quaternary sediments (Archive 1984). Rocks in the source area of debris flow are mainly quartz sandstone and the Zagunao Formation slate. Soft rocks such as slate and sandstone are easily weathered and can provide loose solids for debris flow. Slate and sandstone in some areas are strongly weathered, providing much solid matter for many geological hazards. The lithology of hazards cases in the literature (Peng et al. 2021; Wang et al. 2021; Zhao et al. 2020; Zhu et al. 2021) is mainly slate.

The climate of Jinchuan County is a continental plateau monsoon climate(Malik et al. 2017) which is sunny weather and a significant temperature variation between day and night. The annual average temperature is 27 degrees Celsius, the annual average sunshine is 2129.7 hours, and the frost-free period is 184 days (Fig. 2b). The average yearly precipitation is 616.2 mm and the evaporation is 1500 mm. The climate in the valley is dry. The rainfall in the research area is mainly concentrated in May-September, and maximum rain occurs in June. The cumulative rainfall from May to September in 2020 is 834.1mm. The rainfall is concentrated and abundant.

2.3 The occurrence of debris flow

On July 25, 2020, heavy rain fell on Jinchuan County and its surrounding areas. According to records, the rainfall in Jinchuan County from 8:00 on August 25 to 8:00 on August 26 reached 55.5mm, the most

significant single-day rainfall since 2014. From 8 o'clock on August 11, 2020, to 8 o'clock on August 18, the seven-day accumulated rainfall reached 75.3 mm, and the rainfall on the day of the debris flow outbreak was 17.5 mm (Fig. 3). The single-day rainfall on September 15 was 23.4mm, and the seven-day cumulative rainfall was 27.3mm (Fig. 3).

In the year 2020, Wujia gully experienced three large-scale debris flows and dozens of small-scale debris flows. There had been no debris flow in the preceding 70 years. The debris flow, which occurred on July 25, 2020, was the largest, with a volume of around $1.0\times10^5 m^3$. The accumulation area's mud depth ranged from 1 to 5 meters. It buried a vast area of arable land and caused damaged to six houses. According to the villagers, the transfer was done ahead of time due to a forewarning of impending heavy rain. The enormous, massive sound of the erupting debris flow could be heard for over a long distance.

On August 17, 2020, the next debris flow occurred, dominated by turbulent debris flow. This debris flow broke out and strike multiple times, according to field staff, and lasted several hours. While during the field investigation, it was noted that the debris flow was still moving slowly, and it felt like as if one were standing in a swamp. This real-time expedition assisted in compiling the observed field data.

3 Methodology

3.1 Field investigation and physical experiment

During the field expedition, for compiling the data, the team observed that the third debris flow had slow movements, had a high water content as it crept downwards due to accumulation. The survey of regional natural conditions aimed to collect data on topography and landforms, geological structure, and hydrological surveys, as well as drone photography, resident interviews, and debris flow field sampling. The analysis further included high-resolution topography reconstruction, remote sensing image comparison between before and after the debris flow, traditional soil test, and rheological test. Taking Zengda as a subject, the cause analysis and numerical analysis of debris flow are carried out. As shown in Fig. 4b, two samples were collected at position A, for the macroscopic mechanical properties of debris flow accumulation in order to further examine the fluid material properties of the debris flow.

The slope area provided a major source for the first debris flow in Wujia gully on the northwest side of the channel. The debris flow had a steep slope from the slope to the channel section with an average inclination angle of 40°(Fig. 4a). The upper part of the slope was the primary source material area. Terraces that collect rainwater, primarily cover the vegetation at the rear edge of the source material area.

As shown in Fig. 4c, the distance from the trailing edge to the shear outlet in source material area is about 158m and the maximum width of the source material area is about 43m (Fig. 4c). The average depth of source material shown in Fig. 4c is about 14m and the area of source material is about $5531 m^2$ (Fig. 4c). The average inclination angle of the channel is 17° (Fig. 4a). The accumulation area is $5.2\times10^4 m^{2,}$ and

the average inclination angle is 8° (Fig. 4b). It is mostly cultivated land, with economic crops like pepper being grown.

We collected debris flow samples at the locations marked in the Fig. 4b. The water content and density of the debris flow measured in the experiment can also reflect the water content and density of the debris flow during its movement. According to the ASTM standard (ASTM 1958), the drying method, sieving method, Marvin Nano laser particle size analyzer are used to determine debris flow's moisture content, density, and particle size classification (Table 1). Rheological experiments are conducted on the collected debris flow samples to determine the relationship between shear stress, viscosity coefficient, and shear rate of debris flow samples (Table 1).

Table 1
Physical parameters and its used

Physical parameters	Physical parameters used	Method of obtaining
Water content(%)	Used to determine the density of the slurry	Drying method
Fine particle content after 0.5mm(%)	Used to determine the fine particle content of the slurry	Sieving method
Slurry density ρ(g/cm3)	Configure the slurry density for rheological experiments	Calculate
Bingham yield stress τ_B (Pa)	Used to determine the Bingham yield stress of the numerical simulation	Rheological experiments
Bingham viscosity coefficient μ_B(Pa·s)	Used to determine the Bingham viscosity coefficient of the numerical simulation	Rheological experiments

3.2 Governing equation of numerical method

The 2D debris flow movement model that simplifies Navier-Stokes equation by depth-integrated continuum method is adopted to analyze the debris flows that have occurred dynamic processes in Wujia gully, Zengda, Aba Tibetan and Qiang Autonomous Prefecture, Sichuan Province. Governing equations are presented as:

$$\frac{\partial W}{\partial t}+\frac{\partial F}{\partial x}+\frac{\partial G}{\partial y}=S \qquad (1)$$

in which:

$$W=\begin{bmatrix} h \\ hu \\ hv \end{bmatrix}, F=\begin{bmatrix} hu \\ hu^2+gh^2/2 \\ huv \end{bmatrix}, G=\begin{bmatrix} hu \\ huv \\ hv^2+gh^2/2 \end{bmatrix}, S=\begin{bmatrix} 0 \\ gh(S_{ax}-S_{fx}) \\ gh(S_{ay}-S_{fy}) \end{bmatrix} \quad (2)$$

Where h is flow height, and are the depth-integrated flow velocities in the x and y directions, g is gravitational acceleration, S_{ax} and S_{ay} are the momentum source term in the and directions, S_{fx} and S_{fy} are the resistance term in the and directions, S_{ax} and S_{ay} the format is as follow:

$$S_{ax}=-\frac{\partial Z}{\partial x}, S_{ay}=-\frac{\partial Z}{\partial y} \quad (3)$$

The field investigation shows that the debris flows are viscous. In the process of debris flow simulation, viscous debris flow is usually simplified to the Bingham body model (Julien and Lan 1991; Rickenmann et al. 2006; Ying-Hsin et al. 2013). Therefore, the Bingham body stress constitutive model is used as the resistance model.

The total Bingham friction S_f is as follow:

$$S_f=\frac{\tau_B}{\rho gh}+\frac{K_l\mu_B V}{8\rho gh^2}+\frac{n^2V^2}{h^{4/3}} \quad (4)$$

Where τ_B is the Bingham yield stress; $\mu_B$is the Bingham viscosity; K_l is the laminar flow resistance coefficient; is pseudo-Manning's resistance coefficient; is the depth-averaged velocity which is $\sqrt{u^2+v^2}$; ρ is the fluid density.

The relationship between S_{fx} and S_{fy} and S_f is as follows:

$$S_{fx}=\frac{u}{\sqrt{u^2+v^2}}S_f, S_{fy}=\frac{v}{\sqrt{u^2+v^2}}S_f \quad (5)$$

Massflow solved the depth-integrated continuum governing equation; as Bingham resistance model is not defined in Mass flow, a custom Bingham body resistance simulation is performed for the secondary development of the Massflow. Its robustness has been verified by a series of experimental benchmarks and simulations of actual events. It has been widely used in a variety of two-dimensional surface flow simulation cases (Ouyang et al. 2019a; Ouyang et al. 2015a; Ouyang et al. 2015b; Ouyang et al. 2013; Ouyang et al. 2019b; Ouyang et al. 2016).

4 Result

4.1 Physical experiment results

Knowing to the relationship between the shear rate of the debris flow and the shear stress, the debris flow's stress constitutive model and numerical simulation parameters are determined.

Table 2
Physical parameters of soil in the accumulation

Density ρ(g/cm^3)	Water content (%)	Slurry density ρ(g/cm^3)	Fine particle content after 0.5mm(%)
2.18	12.60	1.75	29.02
Bingham yield stress τ_B(Pa)	Bingham viscosity coefficient μ_B(Pa·s)	Laminar flow resistance coefficient K_l	pseudo- Manning's resistance coefficient n (s·m$^{1/3}$)
4.8688	1.7797	1	0.07

As shown in Table 1, the average density of the two debris flow samples is 2.18 g/cm^3 and water content is 12.60%. The result of two debris flow samples particle size distribution by the sieving method is shown in the Fig. 5a. We can conclude the content of particles with a particle size less than 0.5 mm is 29.02% (Fig. 5a and Table 1). After calculation, the debris flow slurry density is 1.75 g/cm^3(Table 1). Collection of the shear rate and shear force data of two debris flow samples by conducting rheological experiments. The relationship between shear rate and shear stress of debris flow samples is shown as Fig. 5b. We selected Bingham model as the stress constitutive model of debris flow simulation(Cui et al. 2015; Hübl and Steinwendtner 2000, 2001; Whipple 1997). The Bingham body model's yield stress and viscosity coefficient are determined to be 4.8688 Pa and 1.7797 Pa·s (Table 1).

4.2 Debris flow simulation results

Fig. 6 and Fig. 7 shows the flow depth and flow velocity of debris flow movement, respectively. The movement presented in the following time period as t = 0s, the 40s, 70s, 100s, 130s, and 170s. Fig. 6a and Fig. 7a shows the initial state of the debris flow from source material at t = 0s, and the velocity were not activated in Fig. 7a. After a very short time with t=40s, the flow velocity reached 10 m/s in Fig. 7b and the flow depth recorded 8m in Fig. 6b. Fig. 6c-d and Fig. 7c-d shows the debris flow moves towards downstream reached to outlet of the gully with bulbous fronts advance(Iverson et al. 2010b) and the velocity of the debris flow is relatively stable during t=70 and 100s. The velocity at out of the gully recorded the peak averaging 10 m/s and depth of the that massive mass reached 2 to 4 m. The debris flow movement deaccelerated when it merged to the township, Zengda, with average velocity 4 to 6 m/s the depth reduced to 2 m due to its spread over the accumulated area (Fig. 6e-f and Fig. 7e-f) and washed away infrastructure such as roads, houses and farmlands (Fig. 9).

4.3 Analysis of dynamic process

As Fig. 8(a-b) shown, within 10 seconds, the main body of the debris flow has passed through M2. At this stage, the debris flow velocity has reached 17.2m/s (after 10 seconds) and rapidly drops to 0m/s in the next 20 seconds when the debris flow has passed M2 (Fig. 8(a-b), Fig. 6b and Fig. 7b). The debris flow has entered the channel(M3) at 10s (Fig. 8(a-b)), and the fluid depth reaches the maximum at about 20s, about 7.9m, and the velocity has reached 11.9m/s (Fig. 8(a-b)). The debris flow almost wholly passes through the M3 point at the 60s (Fig. 8(a-b), Fig. 6c and Fig. 7c).

The debris flow reached M4–M9 at t=20s, t=30s, t=50s, t=60s, and t=70s((Fig. 8(a-f)). When the debris flow reaches each M4–M9, the velocity is close, then the velocity slowly decreases until the debris flow passes. This shows that the velocity of the debris flow movement in the channel is stable ((Fig. 8(a-f), Fig. 6(b-d) and Fig. 7(b-d)). The debris flow reached M9 at t=90s. The debris flow started to flow out of the channel and began to accumulate ((Fig. 8(e-f), Fig. 6d and Fig. 7d).

The debris flow reached M10–M13 at t=100s, t=120s, t=150s and t=180s((Fig. 8(e-h)), corresponding to the debris flow movement process in Fig. 6(d-f) and Fig. 7(d-f). The flow velocity at this stage does not exceed 5m/s, and is slowly decreasing ((Fig. 8(e-h), Fig. 6(b-d) and Fig. 7(b-d)). At this stage, the debris flow accumulates in the accumulation area as shown in Fig. 9.

4.4 Comparison of simulation result and field evidence

The debris flow arrived at the accumulation area, it formed a depositional area with a north-south distance of 102 meters and an east-west distance of about 512 meters, with an area of about $5.2\times10^4 m^2$ Fig. 9a. When the debris flow moved out of the channel, a house with the height above the foundation of about 6m at the outlet was destroyed by the debris flow Fig. 9b. The debris flow moved downstream, burying a truck that had been destroyed by the debris flow and could no longer be seen in its original shape Fig. 9c. The debris flow also washed away the houses shown in Fig. 9e and Fig. 9f. When the debris flow moved to the location of the house, the first floor of the house was completely buried, whereas the second floor's walls were damaged Fig. 9e and Fig. 9f.

We choose the house shown in Fig. 9e and Fig. 9f as reference points. The debris flow moved to the front of the house and washed away the masonry structure on the second floor of the house. The solid matter of the debris flow was resisted by the house and formed a 5.20m flood level accumulation (Fig. 10e). The debris flow buried the first floor of the house along both sides of the house, and formed a 2m flood level on the back of the house (Fig. 10f). We draw cross-sections for two reference points (Fig. 10b) and extract the simulated flow depth at the front side and back side of the house (Fig. 10c and Fig. 10d). It can be seen that the result between the depth at the reference point and the simulation flow depth cross-section is very close. The average error between the simulated flood level and the observed flood level of the reference point is 0.245m (Fig. 10g).

5 Discussion

5.1 Topography on debris flow moving route

Topography has a significant influence on the movement of debris flow, and various channels also directly shape the movement process of debris flow. There are types of debris flow channels in the world. Typical types of debris flow channels include Y-shaped channels, S-shaped channels, and straight channels. One of the channels named Sanyanyu gully where the Zhouqu debris flow is located is a typical Y-shaped channel(Tang et al. 2011; Wang 2013; Zhang and Matsushima 2016). There is also Jiangjia gully(Chen et al. 2005; Guo et al. 2020; Li et al. 2014; Yong et al. 2012), Niwan gully(Ouyang et al. 2019b), and so on. The S-shaped channel is curved like an S-shaped curve. The representative debris flow events include the Brazilian Brumadinho debris flow (Cambridge and Shaw 2019; Cheng et al. 2021; Du et al. 2020; Esteves et al. 2020; Hussain et al. 2020; Porsani et al. 2019; Silva Rotta et al. 2020; Thompson et al. 2020) and Wenjia gully debris flow{Kang, 2021 #1270;Liu, 2021 #1269;Liu, 2017 #1303;Ni, 2012 #1304;Yu, 2013 #1302;Zhou, 2015 #1306}. The Wujia gully debris flow case selected in this study is a slope debris flow moving in a straight channel, and the channel is very straight. The main channel of Tianmo gully is also a straight channel. The debris flow that broke out in Tianmo gully in 2010 washed away the bridge along the straight channel (Wang et al. 2018; Wei et al. 2018; Zhou et al. 2019).

Figure 11a shows the debris flow moving route; As shown in Fig. 11b, c, the gradient of the slope-channel-accumulation area changes significantly. The moving route of the debris flow, in this case, is ideally explicit. The three topography boundary lines that the moving route passes through are evident. The moving route of the debris flow flows from the slope to the channel, and then flows down the channel into the accumulation area. According to the detailed field investigation and numerical simulation results, the movement trajectory is divided into three parts: slope movement area, channel movement area, and deposition area. The average gradient of the three parts of the topography is 0.85, 0.33, 0.02. The elevation of the movement trajectory is shown in Fig. 11(b).

5.2 Effects of topography on debris flow movement

To describe the change of debris flow during the debris flow movement, we monitored the momentum of all calculation units with non-zero velocity in the simulation. We calculated the average velocity of the debris flow at different times, as shown in Fig. 12. The speed increased sharply in the first 10 seconds, and then decreased in the next 30 seconds, then remained steady for next 60 seconds, and finally the speed gradually decreased. The whole process of debris flow was divided into four stages: acceleration, entering the channel, and deceleration stage, moving smoothly in the channel and slowly accumulating.

The velocity of the fluid is mainly affected by the topography. Fig. 12 shows that the four stages of movement velocity correspond to debris flows to different topography in time. The reason for the acceleration in first stage is because the debris flow flowed on a steep slope. The gradient is large, and the acceleration component provided by gravity is significant. The reason for the deceleration in the

second stage is because the debris flow enters the channel. The gradient of the channel is less than the slope, and the debris flow decelerated when entering the channels. The smooth movement in the third stage is because the debris flow ultimately enters the channel. The gradient of the channel is similar, and the movement speed of the debris flow is relatively stable. The velocity decreased slowly in the fourth stage is that the debris flow entered the accumulation area. The topography of the accumulation area is gentle, the gradient is slight, and the debris flow velocity decreased slowly at this stage and accumulated gradually.

6 Conclusions

On July 25, 2020, a catastrophic debris flow broke out in Wujia gully, Jinchuan County, Sichuan Province, China. Detailed field surveys, laboratory and numerical simulation experiments were conducted to analyze the movement process of Wujia gully debris flow and the influence of topography on the movement process. The results of soil tests and laboratory experiments revealed that the Wujia gully debris flow is a typical viscous debris flow, and the rheological properties of the debris flow are similar to the Bingham fluid. The Bingham yield stress and Bingham viscosity coefficient of debris flow slurry are 4.8688 Pa and 1.7797 Pa·s respectively. The error between the fitted rheological characteristic curve and the rheological experiment result is very small and insignificant.

Based on the findings of field investigation and numerical simulation, it is concluded that topography plays a key role in the movement of Wujia gully debris flow. Particularly in the acceleration, when entering the channel, the deceleration stage, while moving smoothly in the channel and the slowly accumulating stages of the debris flow, which subsequently influenced the risk of the houses downstream. Initially, when debris flow begins in the steep slope movement area, it primarily accelerates in the slope movement area from t=0s to t=10s. Because the gradient of the slope is close to 0.87, the component of gravity in the direction of movement is large due to which the average velocity of the debris flow increases rapidly; Then, the debris flow enters the channel and starts to decelerate. Because the gradient of the channel is smaller than that of the slope, the component force provided by gravity is smaller than that of the slope. Because of the resistance characteristics of Bingham fluid, the velocity of debris flow at this stage is decelerated; Next, the debris flow moves smoothly in the channel. Because the gradient of the channel is similar throughout. The component force of gravity is similar to the resistance, which is similar to inertial motion; Finally, the movement velocity of debris flow in the accumulation zone decreases and accumulates. Because of the low gradient of the accumulation zone, gravity provides almost no component force, mainly due to the resistance of the fluid, this causes the debris flow to gradually slow down and eventually stop.

This research may provide a pathway for analyzing debris flow movement process and as a reference, pave the way for future research on the kinematics of debris flow. The research in this article is important for future debris flow risk assessment and implementation of hazards prevention measures.

Declarations

Acknowledgments

Funding information The study here is funded by Key Research Program of Frontier Sciences，CAS (Grant no.QYZDY-SSW-DQC006), the Major Program of National Natural Science Foundation of China:(Grant no.41790432) and the Strategic Priority Research Program of Chinese Academy of Sciences (Grant no.XDA23090303).

References

1. Ali, S., Haider, R., Abbas, W., Basharat, M. & Reicherter, K. 2021. Empirical assessment of rockfall and debris flow risk along the Karakoram Highway, Pakistan. Natural Hazards, **106**, 2437-2460, doi: 10.1007/s11069-021-04549-4. https://doi.org/10.1007/s11069-021-04549-4
2. Archive, N.G. 1984. *The geology map(Based on the open source data from National Geologycal Archives of China and field investigation.).* **NGA: http://www.ngac.org.cn/**.
3. ASTM, C. 1958. ASTM standards. *Philadelphia: American Society for Testing Materials*.
4. Bhandari, B.P. & Dhakal, S. 2019. Topographical and geological factors on gully-type debris flow in Malai River catchment, Siwaliks, Nepal. Journal of Nepal Geological Society, **59**, 89-94, doi: 103126/jngs.v59i0.24994. https://doi.org/103126/jngs.v59i0.24994
5. Cambridge, M. & Shaw, D. 2019. Preliminary reflections on the failure of the Brumadinho tailings dam in January 2019. Dams and Reservoirs, **29**, 113-123, doi: 10.1680/jdare.19.00004. https://doi.org/10.1680/jdare.19.00004
6. Chang, M., Tang, C., Van Asch, T.W.J. & Cai, F. 2017. Hazard assessment of debris flows in the Wenchuan earthquake-stricken area, South West China. Landslides, **14**, 1783-1792, doi: 10.1007/s10346-017-0824-9. https://doi.org/10.1007/s10346-017-0824-9
7. Chen, C.-Y. & Lee, W.-J. 2010. Topographic features and the initiation of debris flows. *10th Congress INTERPRAEVENT*, 10.
8. Chen, J., He, Y. & Wei, F. 2005. Debris flow erosion and deposition in Jiangjia Gully, Yunnan, China. Environmental Geology, **48**, 771-777, doi: 10.1007/s00254-005-0017-z. https://doi.org/10.1007/s00254-005-0017-z
9. Chen, Y., Qin, S., Qiao, S., Dou, Q., Che, W., Su, G., Yao, J. & Nnanwuba, U.E. 2020. Spatial Predictions of Debris Flow Susceptibility Mapping Using Convolutional Neural Networks in Jilin Province, China. Water, **12**, 2079, doi: 10.3390/w12082079. https://doi.org/10.3390/w12082079
10. Cheng, D., Cui, Y., Li, Z. & Iqbal, J. 2021. Watch Out for the Tailings Pond, a Sharp Edge Hanging over Our Heads: Lessons Learned and Perceptions from the Brumadinho Tailings Dam Failure Disaster. Remote Sensing, **13**, doi: 10.3390/rs13091775. https://doi.org/10.3390/rs13091775

11. Cheng, D., Cui, Y., Su, F., Jia, Y. & Choi, C.E. 2018. The characteristics of the Mocoa compound disaster event, Colombia. Landslides, **15**, 1223-1232, doi: 10.1007/s10346-018-0969-1. https://doi.org/10.1007/s10346-018-0969-1
12. Cui, P., Zeng, C. & Lei, Y. 2015. Experimental analysis on the impact force of viscous debris flow. Earth Surface Processes and Landforms, **40**, 1644-1655, doi: 10.1002/esp.3744. https://doi.org/10.1002/esp.3744
13. Cui, Y.F., Zhou, X.J. & Guo, C.X. 2017. Experimental study on the moving characteristics of fine grains in wide grading unconsolidated soil under heavy rainfall. Journal of Mountain Science, 417-431, doi: 10.1002/esp.3744. https://doi.org/10.1002/esp.3744
14. Dai, F., Lee, C.F., Deng, J. & Tham, L. 2005. The 1786 earthquake-triggered landslide dam and subsequent dam-break flood on the Dadu River, southwestern China. Geomorphology, **65**, 205-221, doi: 10.1016/j.geomorph.2004.08.011. https://doi.org/10.1016/j.geomorph.2004.08.011
15. Dai, Z., Huang, Y., Cheng, H. & Xu, Q. 2017. SPH model for fluid–structure interaction and its application to debris flow impact estimation. Landslides, **14**, 917-928, doi: 10.1007/s10346-016-0777-4. https://doi.org/10.1007/s10346-016-0777-4
16. De Haas, T., Braat, L., Leuven, J.R., Lokhorst, I.R. & Kleinhans, M.G. 2015. Effects of debris flow composition on runout, depositional mechanisms, and deposit morphology in laboratory experiments. Journal of Geophysical Research: Earth Surface, **120**, 1949-1972, doi: 10.1002/2015JF003525. https://doi.org/10.1002/2015JF003525
17. Deng, M., Chen, N. & Liu, M. 2017. Meteorological factors driving glacial till variation and the associated periglacial debris flows in Tianmo Valley, south-eastern Tibetan Plateau. Natural Hazards and Earth System Sciences, **17**, 345-356, doi: 10.5194/nhess-17-345-2017. https://doi.org/10.5194/nhess-17-345-2017
18. Ding, H.R., Li, Y., Ni, S.J., Shao, C.J., Shi, Z.M., Yan, L., Lv, L.Q., Ni, T., Gong, R.H., Shi, L. & Liu, Y.X. 2019. The mountain torrent disasters and its effect on sediment transport after the Wenchuan earthquake. IOP Conference Series: Earth and Environmental Science, **344**, doi: 10.1088/1755-1315/344/1/012159. https://doi.org/10.1088/1755-1315/344/1/012159
19. Du, Z., Ge, L., Ng, A.H., Zhu, Q., Horgan, F.G. & Zhang, Q. 2020. Risk assessment for tailings dams in Brumadinho of Brazil using InSAR time series approach. Sci Total Environ, **717**, 137125, doi: 10.1016/j.scitotenv.2020.137125. https://doi.org/10.1016/j.scitotenv.2020.137125
20. Esteves, G.F., Bressanin, L.A., de Souza, K.R.D., da Silva, A.B., Mantovani, J.R., Marques, D.M., Magalhaes, P.C., Pasqual, M. & de Souza, T.C. 2020. Do tailings from the Mariana, MG (Brazil), disaster affect the initial development of millet, maize, and sorghum? Environ Sci Pollut Res Int, doi: 10.1007/s11356-020-10013-w. https://doi.org/10.1007/s11356-020-10013-w
21. F.C, Dai, and, C.F & Lee. 2002. Landslide characteristics and slope instability modeling using GIS, Lantau Island, Hong Kong. Geomorphology, **42**, 213-228, doi: 10.1016/S0169-555X(01)00087-3. https://doi.org/10.1016/S0169-555X(01)00087-3

22. Guo, X., Li, Y., Cui, P., Yan, H. & Zhuang, J. 2020. Intermittent viscous debris flow formation in Jiangjia Gully from the perspectives of hydrological processes and material supply. Journal of Hydrology, **589**, 125184, doi: 10.1016/j.jhydrol.2020.125184. https://doi.org/10.1016/j.jhydrol.2020.125184
23. Hübl, J. & Steinwendtner, H. 2000. Estimation of rheological properties of viscous debris flow using a belt conveyor. Physics and Chemistry of the Earth, Part B: Hydrology, Oceans and Atmosphere, **25**, 751-755, doi: 10.1016/S1464-1909(00)00097-6. https://doi.org/10.1016/S1464-1909(00)00097-6
24. Hübl, J. & Steinwendtner, H. 2001. Two-dimensional simulation of two viscous debris flows in Austria. Physics and Chemistry of the Earth, Part C: Solar, Terrestrial & Planetary Science, **26**, 639-644, doi: 10.1016/S1464-1917(01)00061-7. https://doi.org/10.1016/S1464-1917(01)00061-7
25. Hussain, Y., Hamza, O., Huang, X., Silva, A.C., Condori, C., Uagoda, R. & Cavalcante, A.L.B. 2020. Seismic signature of mudflow tremor resulted from Brumadinho (Brazil) tailings dam failure. REM - International Engineering Journal, **73**, 421-424, doi: 10.1590/0370-44672019730040. https://doi.org/10.1590/0370-44672019730040
26. Iverson, R.M. 2003. The debris-flow rheology myth. Debris-flow hazards mitigation: mechanics, prediction, and assessment, **1**, 303-314, doi: 10.1.1.722.3486. https://doi.org/10.1.1.722.3486
27. Iverson, R.M. 2005. Debris-flow mechanics. *Debris-flow hazards and related phenomena*. Springer, 105-134.
28. Iverson, R.M. 2015. Scaling and design of landslide and debris-flow experiments. Geomorphology, **244**, 9-20, doi: 10.1016/j.geomorph.2015.02.033. https://doi.org/10.1016/j.geomorph.2015.02.033
29. Iverson, R.M., Logan, M., LaHusen, R.G. & Berti, M. 2010a. The perfect debris flow? Aggregated results from 28 large-scale experiments. Journal of Geophysical Research: Earth Surface, **115**, doi: 10.1029/2009JF001514. https://doi.org/10.1029/2009JF001514
30. Iverson, R.M. & Ouyang, C. 2015. Entrainment of bed material by Earth-surface mass flows: Review and reformulation of depth-integrated theory. Reviews of Geophysics, **53**, 27-58, doi: 10.1002/2013rg000447. https://doi.org/10.1002/2013rg000447
31. Iverson, R.M., Reid, M.E., Logan, M., LaHusen, R.G., Godt, J.W. & Griswold, J.P. 2010b. Positive feedback and momentum growth during debris-flow entrainment of wet bed sediment. Nature Geoscience, **4**, 116-121, doi: 10.1038/ngeo1040. https://doi.org/10.1038/ngeo1040
32. Ji, F., Dai, Z. & Li, R. 2020. A multivariate statistical method for susceptibility analysis of debris flow in southwestern China. Natural Hazards and Earth System Sciences, **20**, 1321-1334, doi: 10.5194/nhess-20-1321-2020. https://doi.org/10.5194/nhess-20-1321-2020
33. Jian, G., Tonglu, L., Ping, L., Xiaoyan, L., Wei, S. & Zhanghui, Z. 2018. A NUMERICAL MODEL FOR SIMULATION OF FLOWSLIDE ON CURVED TOPOGRAPHY. Journal of Engineering Geology, **26**, 319-324(In Chinese).
34. Julien, P.Y. & Lan, Y. 1991. Rheology of hyperconcentrations. Journal of Hydraulic Engineering, **117**, 346-353, doi: 10.1061/(ASCE)0733-9429(1991)117:3(346). https://doi.org/10.1061/(ASCE)0733-9429(1991)117:3(346)

35. Lee, J.S., Song, C.G., Kim, H.T. & Lee, S.O. 2015. Risk analysis considering the topography characteristics of debris flow occurrence area. Journal of the Korean Society of Hazard Mitigation, **15**, 75-82, doi: 10.9798/KOSHAM.2015.15.3.75. https://doi.org/10.9798/KOSHAM.2015.15.3.75
36. Lévy, S., Jaboyedoff, M., Locat, J. & Demers, D. 2012. Erosion and channel change as factors of landslides and valley formation in Champlain Sea Clays: The Chacoura River, Quebec, Canada. Geomorphology, **145**, 12-18, doi: 10.1016/j.geomorph.2011.09.014. https://doi.org/10.1016/j.geomorph.2011.09.014
37. Li, Y., Chen, J., Zhang, Y., Song, S., Han, X. & Ammar, M. 2020. Debris flow susceptibility assessment and runout prediction: a case study in shiyang gully, Beijing, China. International Journal of Environmental Research, **14**, 365-383, doi: 10.1007/s41742-020-00263-4. https://doi.org/10.1007/s41742-020-00263-4
38. Li, Y., Liu, J., Su, F., Xie, J. & Wang, B. 2014. Relationship between grain composition and debris flow characteristics: a case study of the Jiangjia Gully in China. Landslides, **12**, 19-28, doi: 10.1007/s10346-014-0475-z. https://doi.org/10.1007/s10346-014-0475-z
39. Liang, Z., Wang, C.-M. & Zhang, Z.-M. 2020a. A comparison of statistical and machine learning methods for debris flow susceptibility mapping. Stochastic Environmental Research and Risk Assessment, **34**, 1887-1907, doi: 10.1007/s00477-020-01851-8. https://doi.org/10.1007/s00477-020-01851-8
40. Liang, Z., Wang, C., Han, S., Ullah Jan Khan, K. & Liu, Y. 2020b. Classification and susceptibility assessment of debris flow based on a semi-quantitative method combination of the fuzzy C-means algorithm, factor analysis and efficacy coefficient. Natural Hazards and Earth System Sciences, **20**, 1287-1304, doi: 10.5194/nhess-20-1287-2020. https://doi.org/10.5194/nhess-20-1287-2020
41. Liu, X., Shu, X., Liu, X., Duan, Z. & Ran, Z. 2020. Risk Assessment of Debris Flow in Ya'an City Based on BP Neural Network. *IOP Conference Series: Materials Science and Engineering*. IOP Publishing, 012006.
42. Malik, I., Wistuba, M., Tie, Y., Owczarek, P., Woskowicz-Ślęzak, B. & Łuszczyńska, K. 2017. Mass movements of differing magnitude and frequency in a developing high-mountain area of the Moxi basin, Hengduan Mts, China–A hazard assessment. Applied geography, **87**, 54-65, doi: 10.1016/j.apgeog.2017.08.003. https://doi.org/10.1016/j.apgeog.2017.08.003
43. Minatti, L. & Pasculli, A. 2011. SPH numerical approach in modelling 2D muddy debris flow. *International Conference on Debris-Flow Hazards Mitigation: Mechanics, Prediction, and Assessment, Proceedings*, 467-475.
44. Ni, H., Zheng, W., Song, Z. & Xu, W. 2014. Catastrophic debris flows triggered by a 4 July 2013 rainfall in Shimian, SW China: formation mechanism, disaster characteristics and the lessons learned. Landslides, **11**, 909-921, doi: 10.1007/s10346-014-0514-9. https://doi.org/10.1007/s10346-014-0514-9
45. Ouyang, C., An, H., Zhou, S., Wang, Z., Su, P., Wang, D., Cheng, D. & She, J. 2019a. Insights from the failure and dynamic characteristics of two sequential landslides at Baige village along the Jinsha

River, China. Landslides, **16**, 1397-1414, doi: 10.1007/s10346-019-01177-9. https://doi.org/10.1007/s10346-019-01177-9

46. Ouyang, C., He, S. & Tang, C. 2015a. Numerical analysis of dynamics of debris flow over erodible beds in Wenchuan earthquake-induced area. Engineering Geology, **194**, 62-72, doi: 10.1016/j.enggeo.2014.07.012. https://doi.org/10.1016/j.enggeo.2014.07.012
47. Ouyang, C., He, S. & Xu, Q. 2015b. MacCormack-TVD Finite Difference Solution for Dam Break Hydraulics over Erodible Sediment Beds. Journal of Hydraulic Engineering, **141**, doi: 10.1061/(asce)hy.1943-7900.0000986. https://doi.org/10.1061/(asce)hy.1943-7900.0000986
48. Ouyang, C., He, S., Xu, Q., Luo, Y. & Zhang, W. 2013. A MacCormack-TVD finite difference method to simulate the mass flow in mountainous terrain with variable computational domain. Computers & Geosciences, **52**, 1-10, doi: 10.1016/j.cageo.2012.08.024. https://doi.org/10.1016/j.cageo.2012.08.024
49. Ouyang, C., Wang, Z., An, H., Liu, X. & Wang, D. 2019b. An example of a hazard and risk assessment for debris flows—A case study of Niwan Gully, Wudu, China. Engineering Geology, **263**, doi: 10.1016/j.enggeo.2019.105351. https://doi.org/10.1016/j.enggeo.2019.105351
50. Ouyang, C., Zhou, K., Xu, Q., Yin, J., Peng, D., Wang, D. & Li, W. 2016. Dynamic analysis and numerical modeling of the 2015 catastrophic landslide of the construction waste landfill at Guangming, Shenzhen, China. Landslides, **14**, 705-718, doi: 10.1007/s10346-016-0764-9. https://doi.org/10.1007/s10346-016-0764-9
51. Peng, J., Fan, Z., Wu, D., Zhuang, J. & Zhao, C. 2014. Heavy rainfall triggered loess-mudstone landslide and subsequent debris flow in Tianshui, China. Engineering Geology, **186**, doi: 10.1016/j.enggeo.2014.08.015. https://doi.org/10.1016/j.enggeo.2014.08.015
52. Peng, T., Chen, N., Hu, G., Tian, S., Han, Z. & Liu, E. 2021. New insights into the delayed initiation of a debris flow in southwest China. Natural Hazards, 1-23, doi: 10.1007/s11069-021-04803-9. https://doi.org/10.1007/s11069-021-04803-9
53. Porsani, J.L., Jesus, F.A.N.d. & Stangari, M.C. 2019. GPR Survey on an Iron Mining Area after the Collapse of the Tailings Dam I at the Córrego do Feijão Mine in Brumadinho-MG, Brazil. Remote Sensing, **11**, doi: 10.3390/rs11070860. https://doi.org/10.3390/rs11070860
54. Preuth, T., Glade, T. & Demoulin, A. 2010. Stability analysis of a human-influenced landslide in eastern Belgium. Geomorphology, **120**, 38-47, doi: 10.1016/j.geomorph.2009.09.013. https://doi.org/10.1016/j.geomorph.2009.09.013
55. Reid, M.E., Iverson, R.M., Logan, M., LaHusen, R.G., Godt, J.W. & Griswold, J.P. 2011. Entrainment of bed sediment by debris flows: results from large-scale experiments. *Fifth International Conference on Debris-flow Hazards Mitigation, Mechanics, Prediction and Assessment, edited by: R. Genevois, Hamilton, DL, and Prestinizi, A., Casa Editrice Universita La Sapienza, Rome*. Citeseer, 367-374.
56. Rickenmann, D., Laigle, D., McArdell, B.W. & Hübl, J. 2006. Comparison of 2D debris-flow simulation models with field events. Computational Geosciences, **10**, 241-264, doi: 10.1007/s10596-005-9021-3. https://doi.org/10.1007/s10596-005-9021-3

57. Shen, W., Zhao, T., Zhao, J., Dai, F. & Zhou, G.G. 2018. Quantifying the impact of dry debris flow against a rigid barrier by DEM analyses. Engineering Geology, **241**, 86-96, doi: 10.1016/j.enggeo.2018.05.011. https://doi.org/10.1016/j.enggeo.2018.05.011
58. Silva Rotta, L.H., Alcântara, E., Park, E., Negri, R.G., Lin, Y.N., Bernardo, N., Mendes, T.S.G. & Souza Filho, C.R. 2020. The 2019 Brumadinho tailings dam collapse: Possible cause and impacts of the worst human and environmental disaster in Brazil. International Journal of Applied Earth Observation and Geoinformation, **90**, doi: 10.1016/j.jag.2020.102119. https://doi.org/10.1016/j.jag.2020.102119
59. Statistics, N.B.o. 2020. Zengda Township.
60. Sujatha, E.R. 2020. A spatial model for the assessment of debris flow susceptibility along the Kodaikkanal-Palani traffic corridor. Frontiers of Earth Science, 1-18, doi: 10.1007/s11707-019-0775-7. https://doi.org/10.1007/s11707-019-0775-7
61. Tang, C., Rengers, N.v., Van Asch, T.W., Yang, Y. & Wang, G. 2011. Triggering conditions and depositional characteristics of a disastrous debris flow event in Zhouqu city, Gansu Province, northwestern China. Natural Hazards and Earth System Sciences, **11**, 2903-2912, doi: 10.5194/nhess-11-2903-2011. https://doi.org/10.5194/nhess-11-2903-2011
62. Thompson, F., de Oliveira, B.C., Cordeiro, M.C., Masi, B.P., Rangel, T.P., Paz, P., Freitas, T., Lopes, G., Silva, B.S., A, S.C., Soares, M., Lacerda, D., Dos Santos Vergilio, C., Lopes-Ferreira, M., Lima, C., Thompson, C. & de Rezende, C.E. 2020. Severe impacts of the Brumadinho dam failure (Minas Gerais, Brazil) on the water quality of the Paraopeba River. Sci Total Environ, **705**, 135914, doi: 10.1016/j.scitotenv.2019.135914. https://doi.org/10.1016/j.scitotenv.2019.135914
63. Tie, Y. 2014. Topographic Features of Debris Flow Gullies in Moxi Basin, Southwestern of China. Journal of Geoscience and Environment Protection, **02**, 27-34, doi: 10.4236/gep.2014.23004. https://doi.org/10.4236/gep.2014.23004
64. Vanmaercke, M., Zenebe, A., Poesen, J., Nyssen, J., Verstraeten, G. & Deckers, J. 2010. Sediment dynamics and the role of flash floods in sediment export from medium-sized catchments: a case study from the semi-arid tropical highlands in northern Ethiopia. Journal of Soils & Sediments, **10**, 611-627, doi: 10.1007/s11368-010-0203-9. https://doi.org/10.1007/s11368-010-0203-9
65. Wang, G. 2013. Lessons learned from protective measures associated with the 2010 Zhouqu debris flow disaster in China. Natural Hazards, **69**, 1835-1847, doi: 10.1007/s11069-013-0772-1. https://doi.org/10.1007/s11069-013-0772-1
66. Wang, J., Cui, Y., Choi, C.E. & Ng, C.W. 2018. The effect of climate change on alpine mountain hazards chain: A case study in Tianmo Ravine, Tibet, China. *The International Congress on Environmental Geotechnics*. Springer, 461-470.
67. Wang, Q., Cheng, C., Agathokleous, E., Zang, S. & Sheng, X. 2021. Bacterial communities in habitats of Dongchuan, China: Their role in slate weathering in triggering and flowing areas of debris flow. doi: 10.21203/rs.3.rs-417585/v1. https://doi.org/10.21203/rs.3.rs-417585/v1

68. Wei, R., Zeng, Q., Davies, T., Yuan, G., Wang, K., Xue, X. & Yin, Q. 2018. Geohazard cascade and mechanism of large debris flows in Tianmo gully, SE Tibetan Plateau and implications to hazard monitoring. Engineering Geology, **233**, 172-182, doi: 10.1016/j.enggeo.2017.12.013. https://doi.org/10.1016/j.enggeo.2017.12.013
69. Whipple, K.X. 1997. Open-channel flow of Bingham fluids: applications in debris-flow research. The Journal of Geology, **105**, 243-262, doi: 10.1086/515916. https://doi.org/10.1086/515916
70. Wu, Y., Liu, X., Wang, J.a., Liu, L. & Shi, P. 2016. Landslide and Debris Flow Disasters in China. *Natural Disasters in China*, 73-101.
71. Xiao, Q.C., Peng, C., Yong, L. & Wan, Y.Z. 2011. Emergency response to the Tangjiashan landslide-dammed lake resulting from the 2008 Wenchuan Earthquake, China. Landslides, **8**, 91-98, doi: 10.1007/s10346-010-0236-6. https://doi.org/10.1007/s10346-010-0236-6
72. Xiong, K., Adhikari, B.R., Stamatopoulos, C.A., Zhan, Y., Wu, S., Dong, Z. & Di, B. 2020. Comparison of different machine learning methods for debris flow susceptibility mapping: A case study in the Sichuan Province, China. Remote Sensing, **12**, 295, doi: 10.3390/rs12020295. https://doi.org/10.3390/rs12020295
73. Ying-Hsin, Wu, Ko-Fei, Liu, Yi-Chin & Chen. 2013. Comparison between FLO-2D and Debris-2D on the application of assessment of granular debris flow hazards with case study. Journal of Mountain Science, doi: 10.1007/s11629-013-2511-1. https://doi.org/10.1007/s11629-013-2511-1
74. Yong, L., Jingjing, L., Kaiheng, H. & Pengcheng, S. 2012. Probability distribution of measured debris-flow velocity in Jiangjia Gully, Yunnan Province, China. Natural Hazards, **60**, 689-701, doi: 10.1007/s11069-011-0033-0. https://doi.org/10.1007/s11069-011-0033-0
75. Zhang, N. & Matsushima, T. 2016. Simulation of rainfall-induced debris flow considering material entrainment. Engineering Geology, **214**, 107-115, doi: 10.1016/j.enggeo.2016.10.005. https://doi.org/10.1016/j.enggeo.2016.10.005
76. Zhao, Y., Meng, X., Qi, T., Qing, F., Xiong, M., Li, Y., Guo, P. & Chen, G. 2020. AI-based identification of low-frequency debris flow catchments in the Bailong River basin, China. Geomorphology, **359**, 107125, doi: 10.1016/j.geomorph.2020.107125. https://doi.org/10.1016/j.geomorph.2020.107125
77. Zhou, G.G., Chen, L.-l., Mu, Q.-y., Cui, K.F.E. & Song, D.-r. 2019. Effects of water content on the shear behavior and critical state of glacial till in Tianmo Gully of Tibet, China. Journal of Mountain Science, **16**, 1743-1759, doi: 10.1007/s11629-019-5440-9. https://doi.org/10.1007/s11629-019-5440-9
78. Zhu, L., He, S., Qin, H., He, W., Zhang, H., Zhang, Y., Jian, J., Li, J. & Su, P. 2021. Analyzing the multi-hazard chain induced by a debris flow in Xiaojinchuan River, Sichuan, China. Engineering Geology, 106280, doi: 10.1016/j.enggeo.2021.106280. https://doi.org/10.1016/j.enggeo.2021.106280

Figures

Figure 1

Location of the Wujia gully in Zengda, Dadu River Basin, China. (a) Location within China. (b) Location within Dadu River Basin. (c) Location of Wujia gully within Zengda

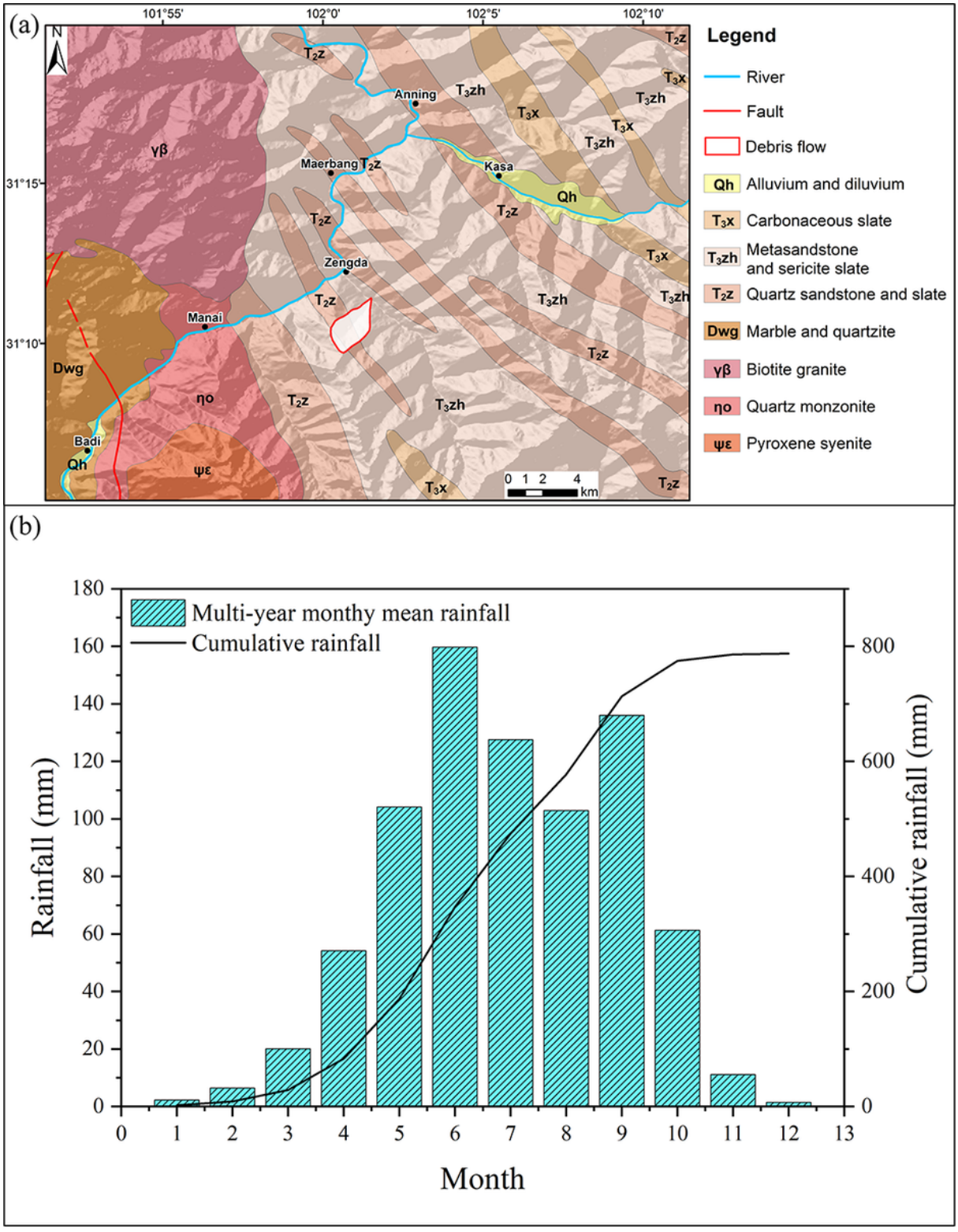

Figure 2

(a) Geological structure and lithologic distribution in the study area. (b) Average monthly precipitation data for the study area.

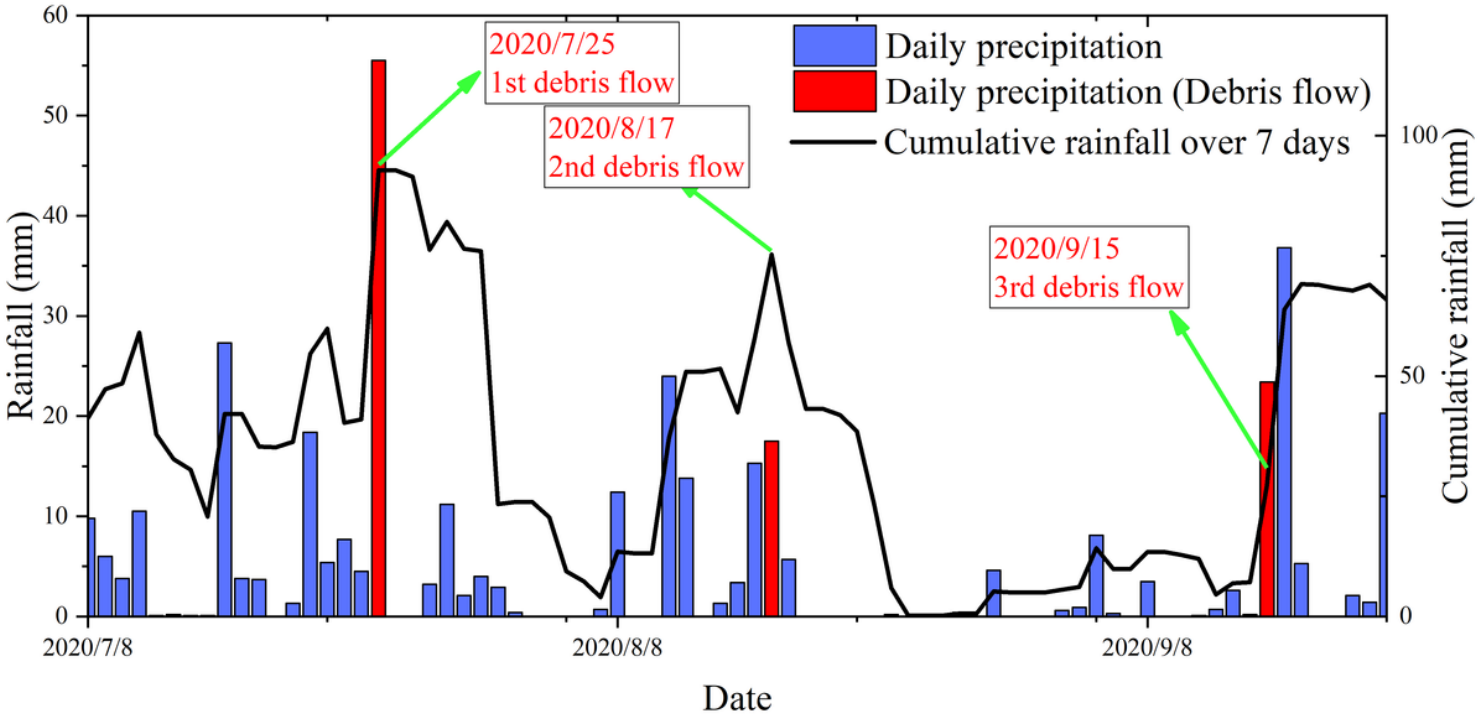

Figure 3

The daily precipitation in Zengda town before September 22 (data from Sichuan Provincial Meteorological Service)

Figure 4

Remote sensing image and UAV images of Wujia gully debris flow. (a) The spatial relationship between Wujia gully and Zengda. (b) Three times debris flows accumulation. (c) Sourec area in Wujia gully

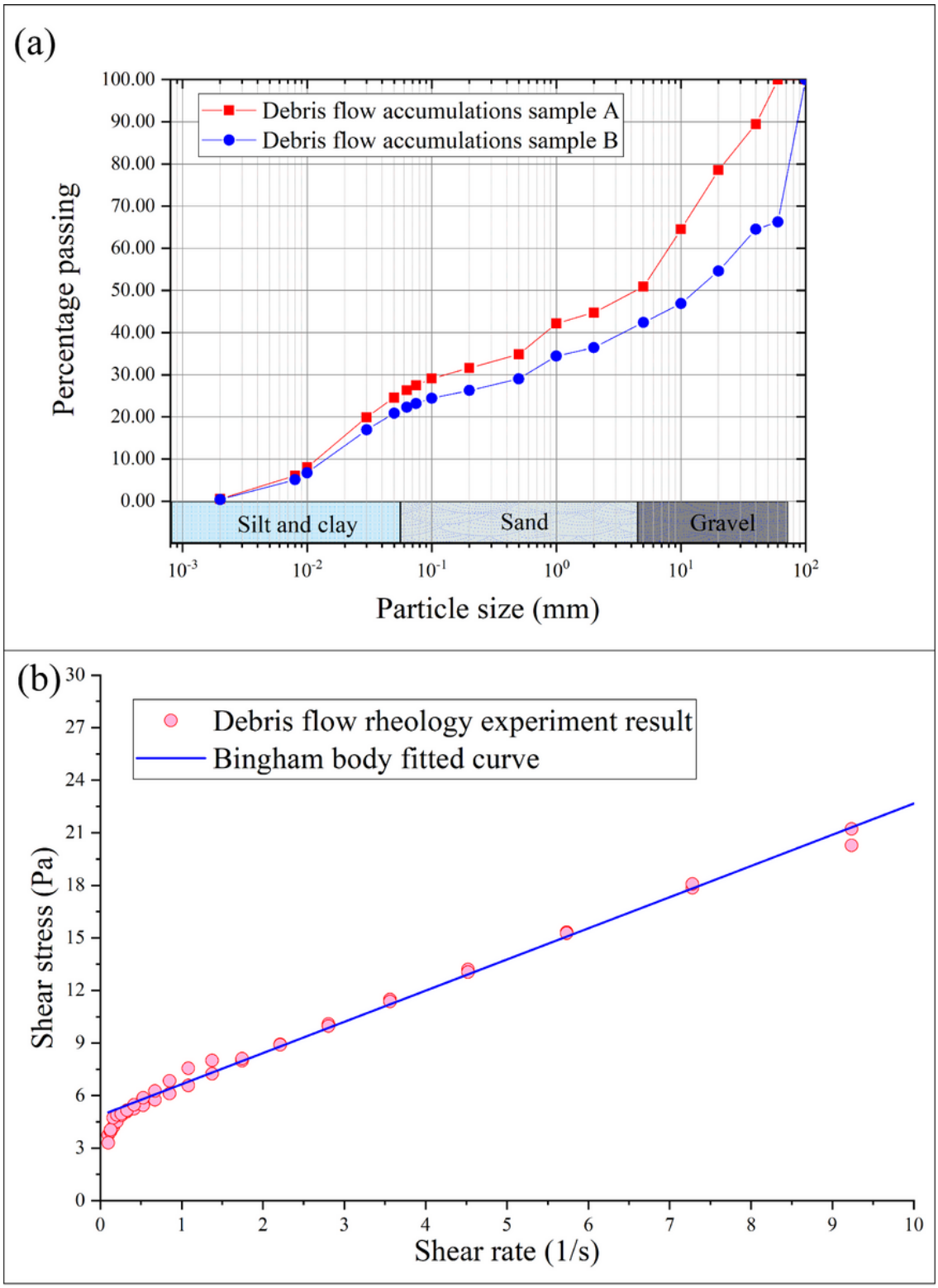

Figure 5

(a) Particle size distribution of debris-flow deposits in Wujia gully. (b) rheological experiments samples and fitted result

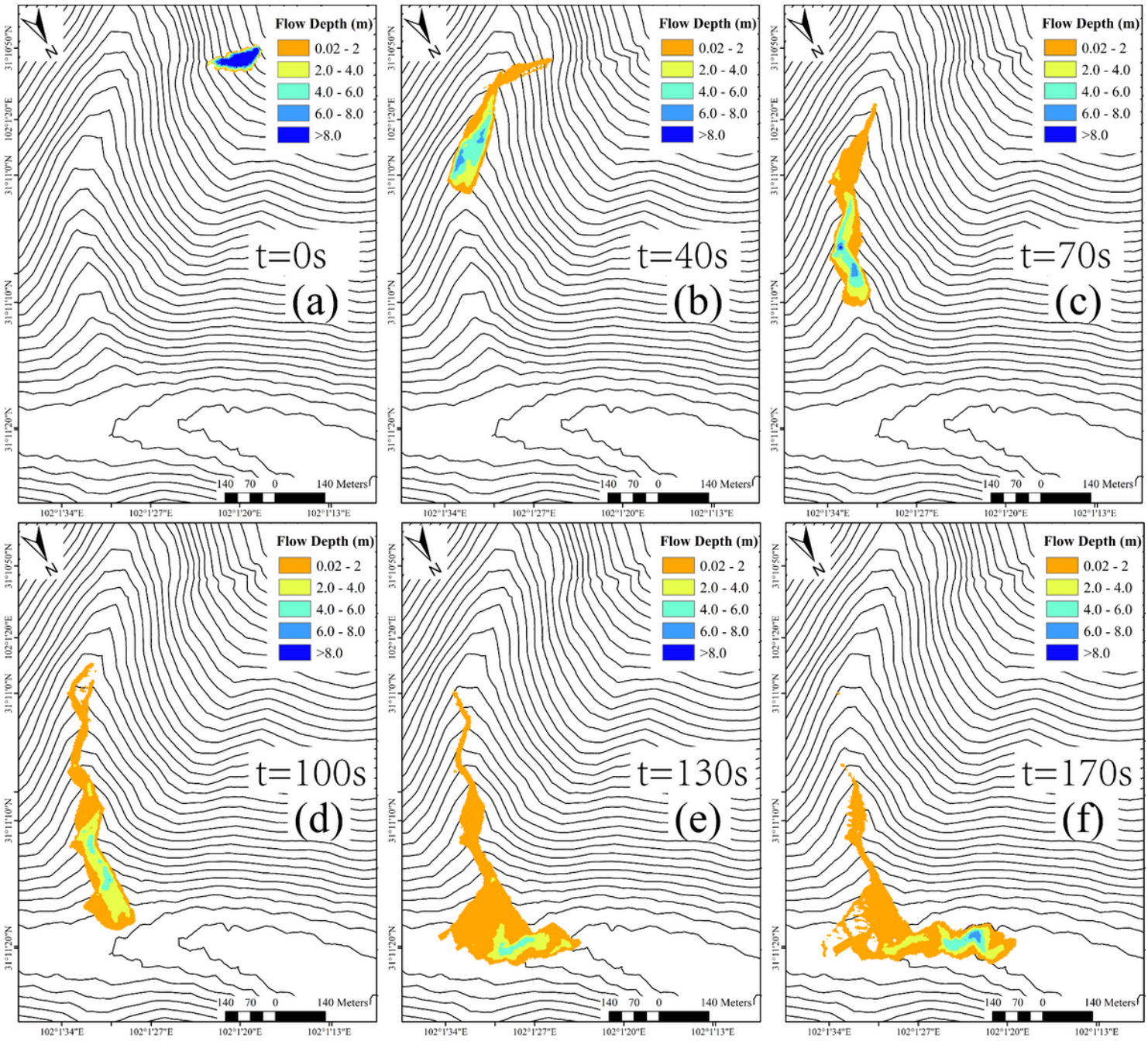

Figure 6

Snapshots of the computed flow height contours of the debris flow at (a) t = 0s, (b) t = 40s, (c) t =70s, (d) t =100s, (e) t =130s, and (f) t =170s

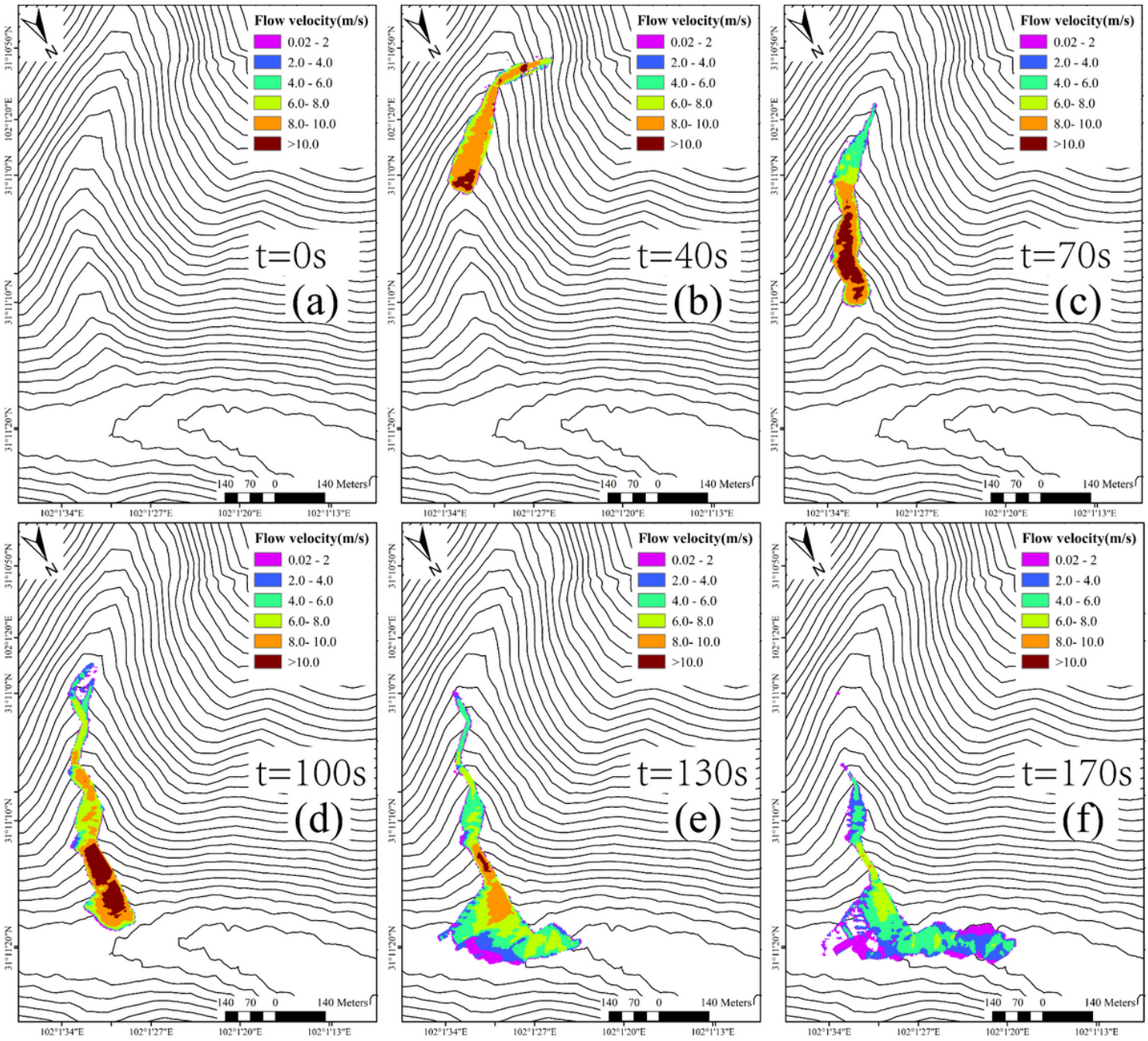

Figure 7

Snapshots of the computed flow velocity contours of the debris flow at (a) t = 0s, (b) t = 40s, (c) t =70s, (d) t =100s, (e) t =130s, and (f) t =170s

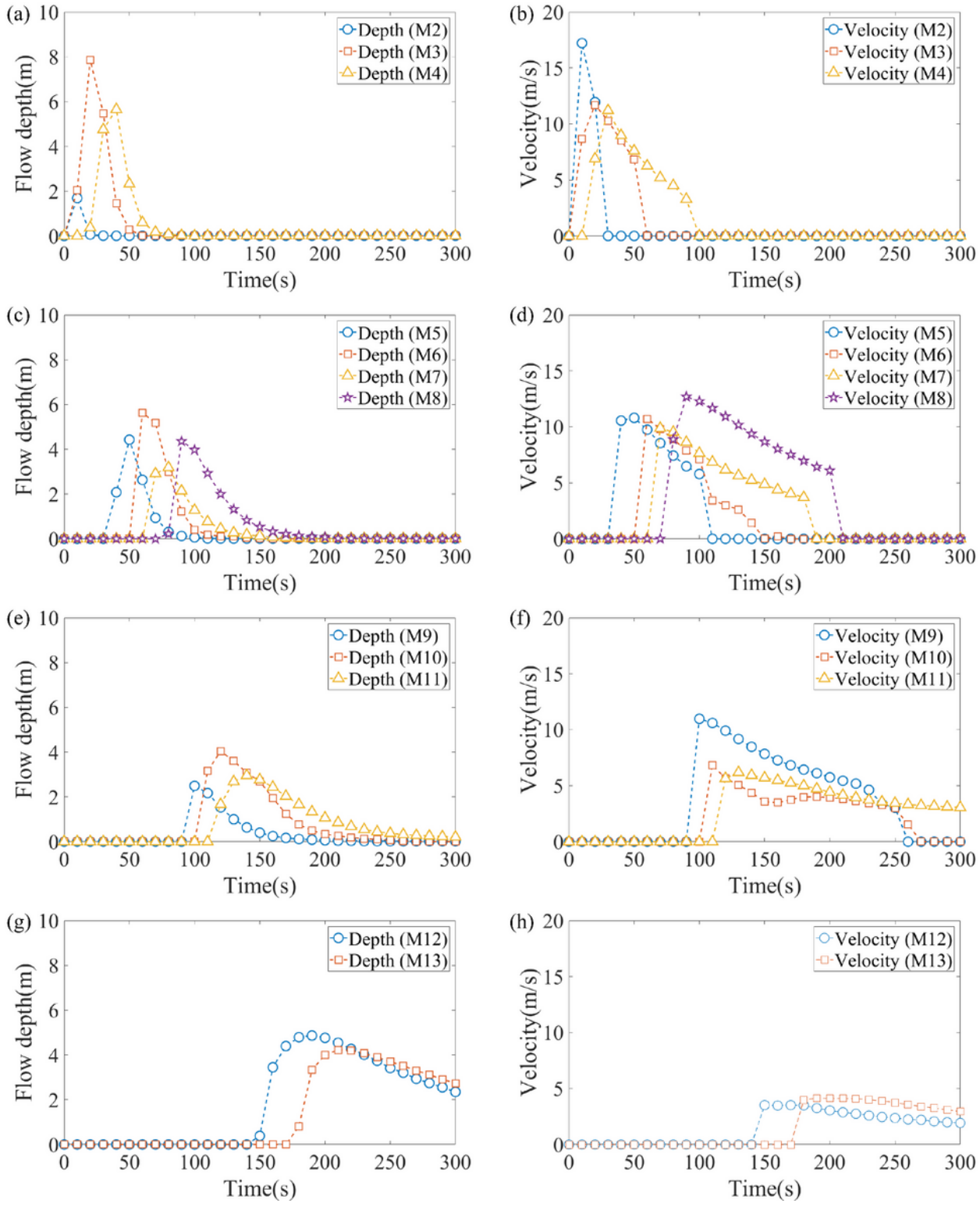

Figure 8

(a-b) Variation in depth and velocity in the slope area (M2–M4). (c-d) Variation in depth and velocity in the channel movement area (M5–M8). (e-f) Variation in depth and velocity in downstream the area (M9–M11). (g-h) Variation in depth and velocity in accumulation area (M12–M13)

Figure 9

Details in the debris flow accumulation area. (a) Debris flow accumulation area. (b) Half of the house was cut. (c) The truck was destroyed by the debris flow and could hardly see its original shape. (d) Debris flow creeps slowly on the field. (e) A house was destroyed by debris flow in the accumulation area(The front side). (f) A house destroyed by debris flow in the accumulation area(The back side).

Figure 10

Comparison of simulation result and field observation. (a) Debris flow accumulation area and reference point. (b) simulation flood level and cross-section. (c) Simulation flood level cross-section A and reference point A observe data. (d) Simulation flood level cross-section B and reference point B observe data. (e) Reference point A simulation flood level and observe flood level. (f) Reference point B simulation flood level and observe flood level. (f) Reference point B and Reference point A flood level comparison.

Figure 11

(a) Monitor points and debris flow moving route. (b) Topographic profile of moving route. (c) Gradient of moving route

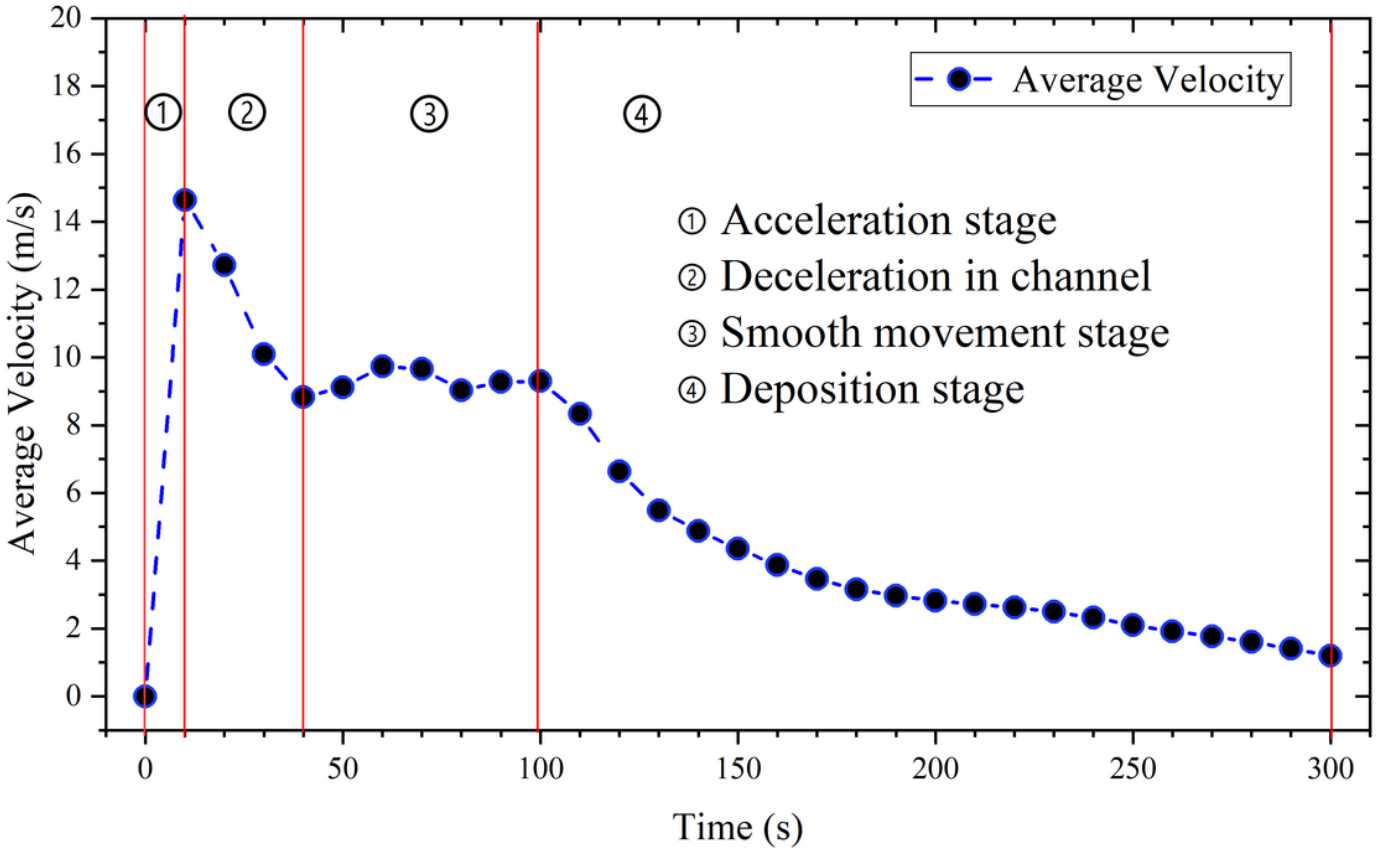

Figure 12

Average velocity of the debris flow movement by numerical simulation